

## Supplementary Figures

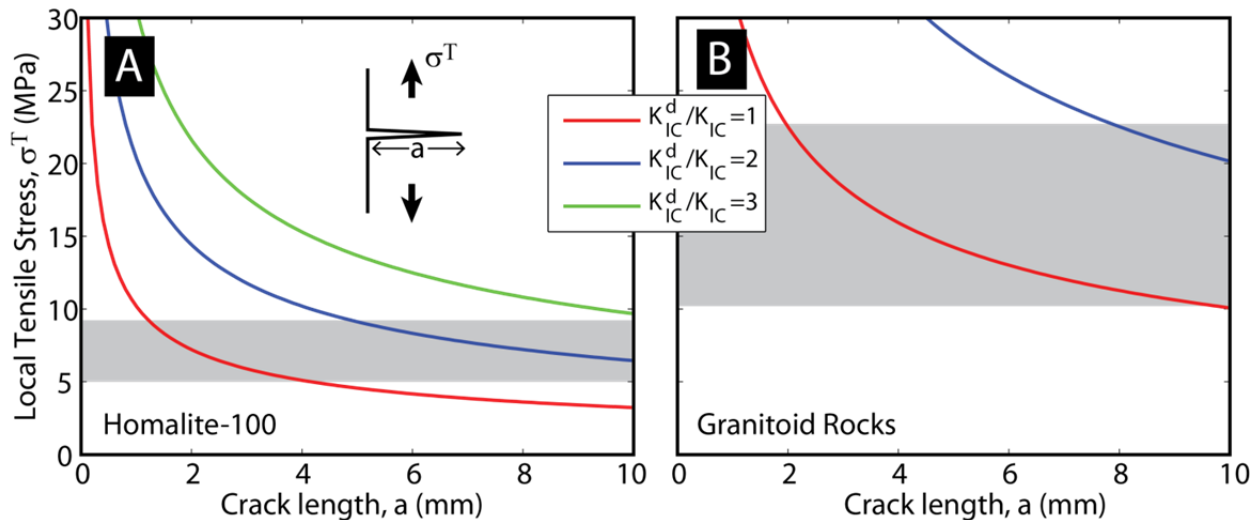


Figure DR1: The critical stress intensity factors for propagating cracks in Homalite 100 can be estimated from data collected by Kobayashi and Dally (1977), who determined the dynamic fracture toughness of Homalite-100 as a function of both plate thickness and of crack speed. The quasi-static fracture toughness ( $K_{IC}$ ) for a Homalite-100 plate of thickness 9.5 mm (equal to the plate thickness in Griffith et al., 2009) is  $0.64 \text{ MPa m}^{1/2}$ . The dynamic fracture toughness ( $K_{IC}^d$ ) deviates from  $K_{IC}$  only above a critical crack velocity ( $\sim 0.25c_s$ ) at which point crack branching is observed (Kobayashi and Dally, 1977). The crack speeds of the tensile microcracks in the experiments by Griffith et al. (2009) were near or below this critical speed, and no branching was observed in the experiments. In view of this, we assume that crack propagation in the tensile zone behind the rupture tip occurs when the critical stress intensity factor is nearly equal to the quasi-static fracture toughness, i.e.  $K_{IC}^d / K_{IC} \approx 1$ . Furthermore, in order to estimate the limiting tensile stress for crack arrest at a distance  $l_c$  behind the rupture tip, we assume that for arrested microcracks,  $K_I = K_{IC}^d(a, v = 0) \approx K_{IC}$ . This assumption allows us to use the functional relationship between the stress intensity factor  $K_I$ , the local crack normal tensile stress  $\sigma$ , and the microcrack length  $a$ , for an edge crack in a semi-infinite plate, i.e.  $K_I = 1.12\sigma^T\sqrt{\pi a}$  (Tada et al., 1985), to estimate the limiting tensile stress,  $\sigma^T$ , at microcrack arrest. Based on the experimental observations of the average “peak” crack length  $a$  (found to range from 2 to 5mm) in the tensile zone behind the rupture tip, we estimate the critical local tensile stress necessary for micro-crack growth to be  $\sim 5 \text{ MPa}$ . The value of  $10 \text{ MPa}$  is estimated for the critical tensile stress threshold for granitoid rocks based on  $K_{IC} \approx 2 \text{ MPa m}^{1/2}$  (e.g., Meredith and Atkinson, 1987)

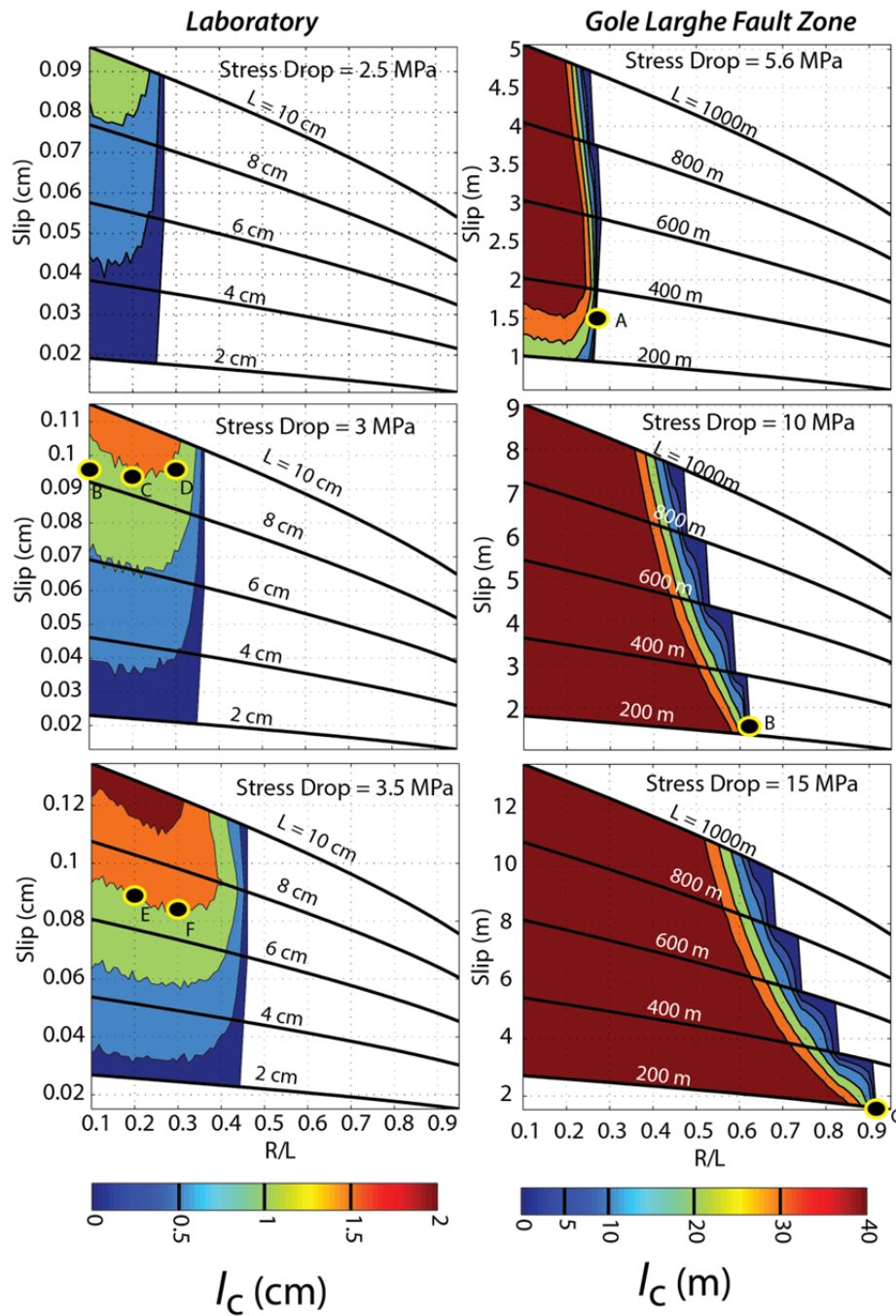


Figure DR2: Predictions of  $l_c$  (color contours) for different combinations of Slip,  $R$ , and  $L$  for laboratory experiments (A-C) and the Gole Larghe Fault Zone (D-F). Each plot represents a single dynamic stress drop value. Yellow circles labeled B-F in the left column represent stress fields depicted in DR4-6, and yellow circles labeled A-C represent stress fields depicted in DR7. In left column, measured  $l_c$  in experiments is approximately 1.5 cm and in D-F,  $l_c$  is expected to be less than 6m (see main text for discussion). The relationship between slip and  $R/L$  for each value of  $L$  is based on equation A21 in Rice et al. (2005) for the total locked in displacement during the slip pulse.

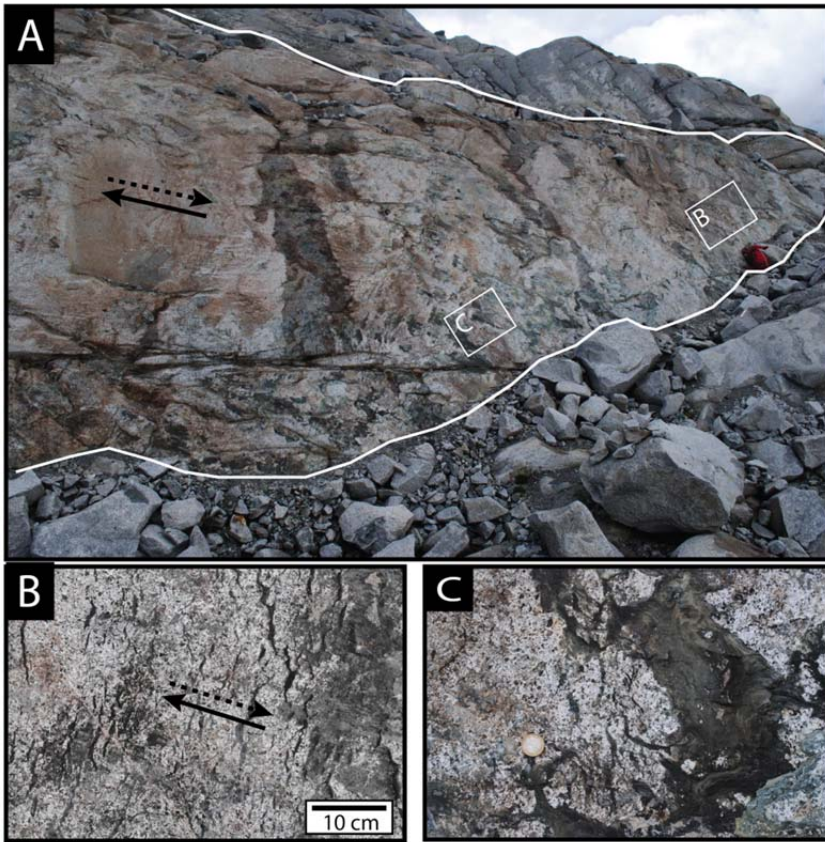


Figure DR3: Outcrop of footwall block fault surface in the GLFZ showing locations of (B) and (C). Red backpack for scale. Slip direction evidenced by slickenlines is consistent across the outcrop and is shown by orientation of arrows on the left side of the picture. (B) Base of Injection veins growing into footwall block as exposed on fault surface. Injection veins as shown in (B) occur in patches along the fault surface. (C) Pseudotachylyte fault vein shown as a patch of pseudotachylyte, covering a few injection veins. The rest of the fault surface at this location is free of injection veins. One Euro coin for scale.

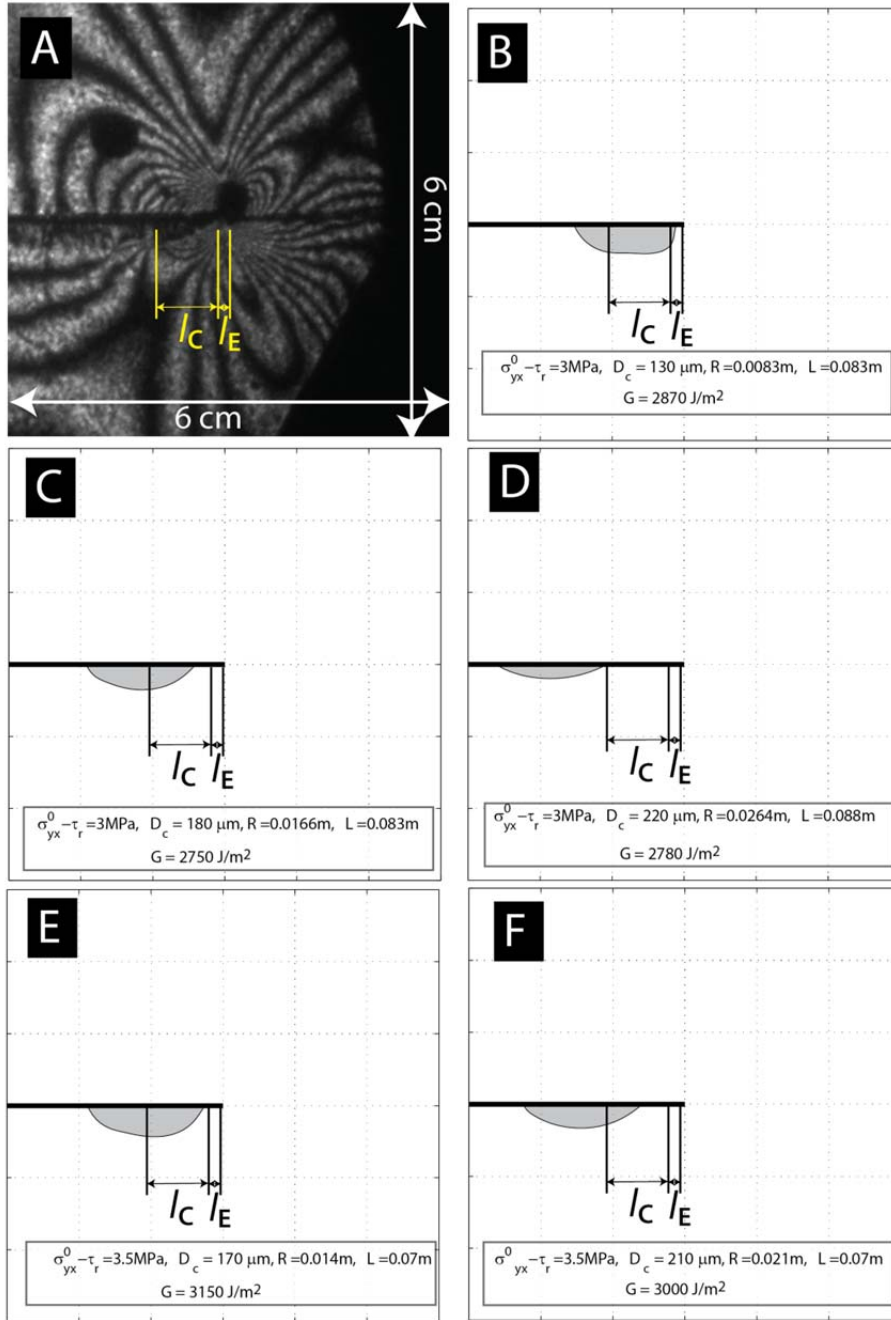


Figure DR4. Comparison between observed  $l_c$  in experiment and predicted  $l_c$  by the slip pulse model. Arrows depicting the length of  $l_c$  and  $l_E$  in each plot are taken from experimental observations (A), whereas the gray area for each set of parameters corresponds to the region in which the crack-perpendicular tensile stress  $\sigma_T$  exceeds 5MPa, as determined in Figure DR1A. Parameter combination in B provides the best fit to experimental observations in terms of the position of the tensile zone with respect to the rupture tip. This conclusion is confirmed in Figures 3, DR5 and DR6. Each plot is 6cm x 6 cm.

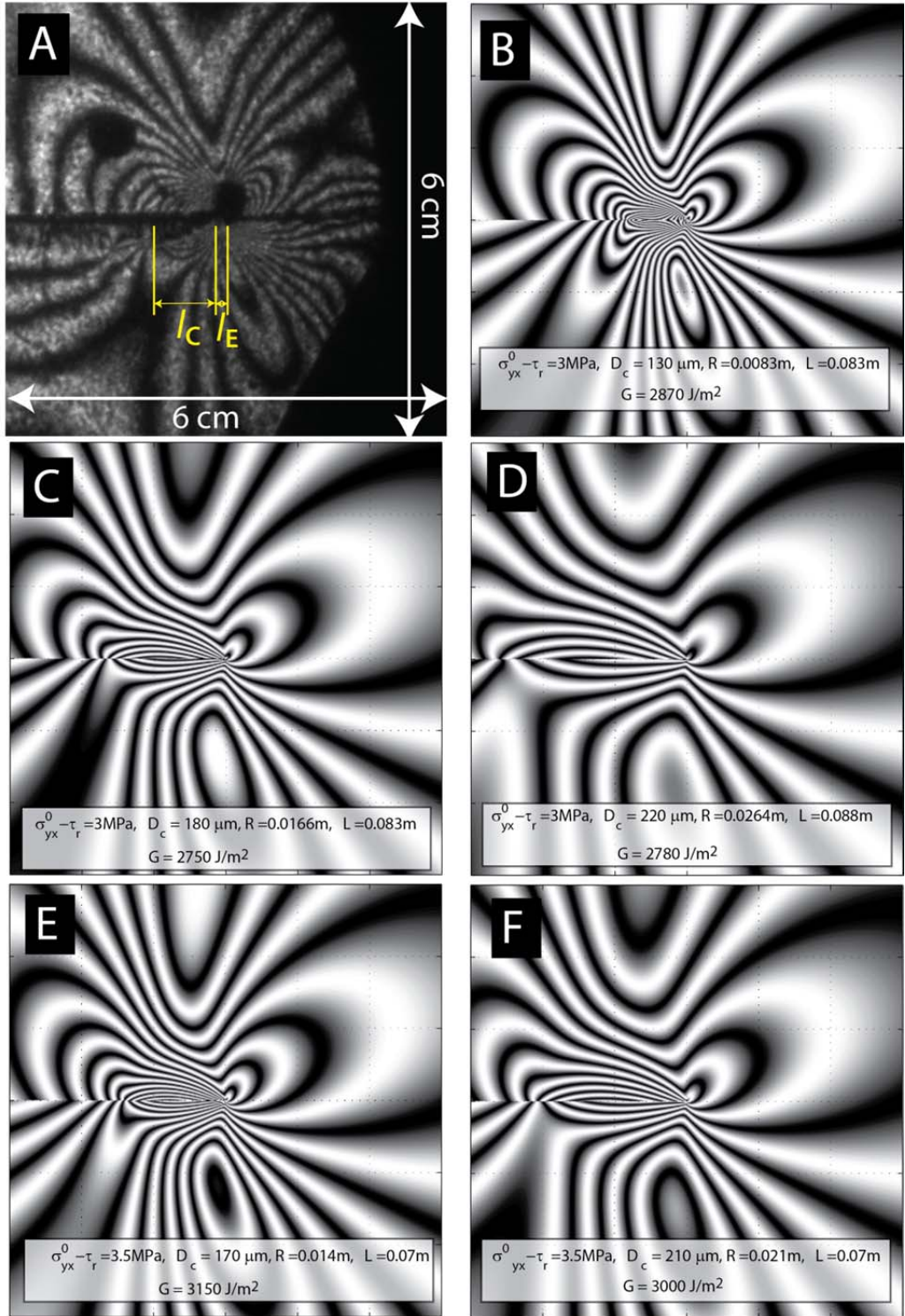


Figure DR5. Comparison of near-tip fringe patterns for all parameter combinations shown in Figure DR4. Each plot is 6cm x 6 cm.

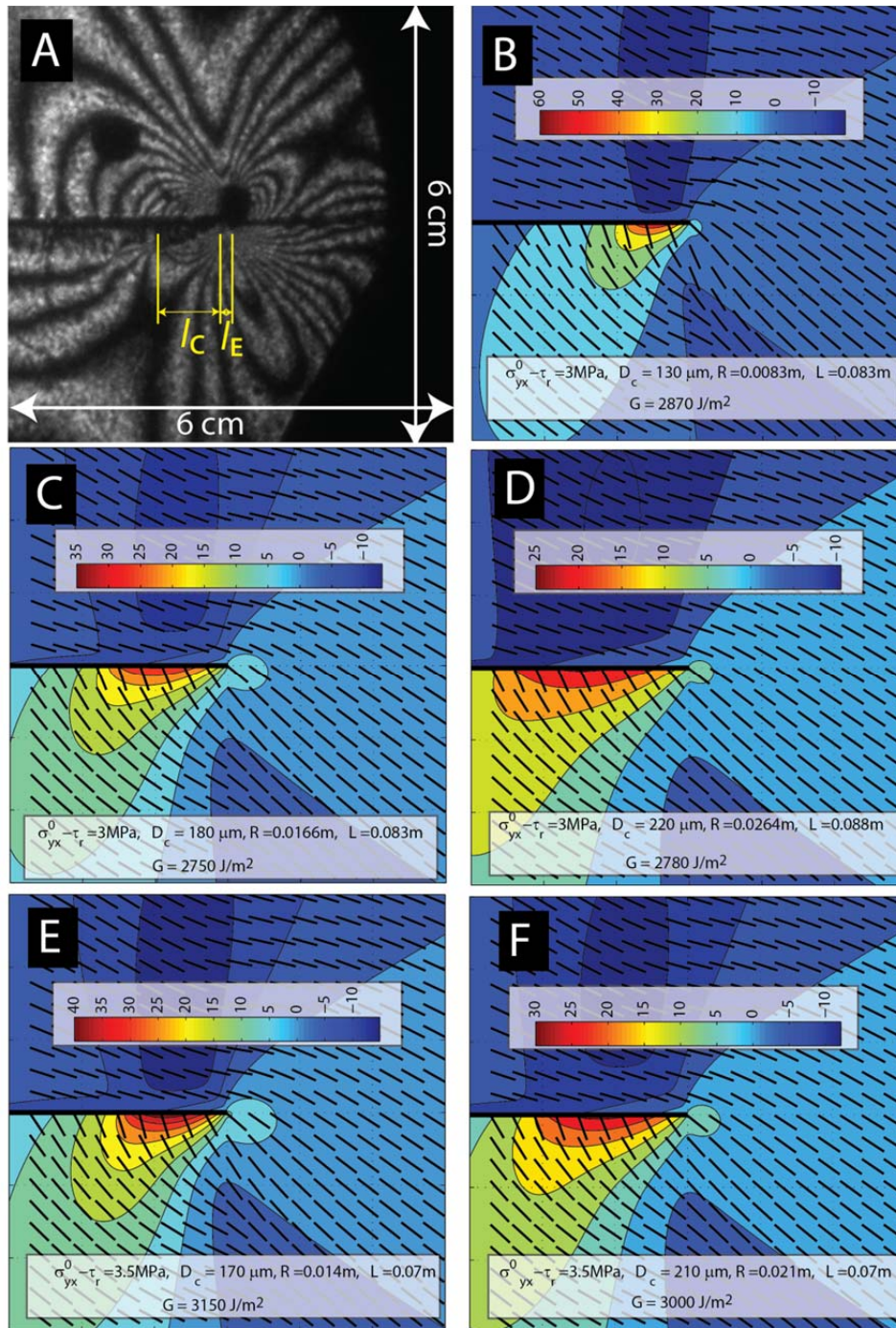


Figure DR6: Near tip contours of maximum tensile stress (units in MPa) during laboratory experiments showing trajectories of maximum compressive stress for experiment 60I of Griffith et al. (2009). Values of dynamic stress drop, peak tensile stress,  $L$ , and  $R$  are shown at the bottom of each plot. Rupture velocity  $v_{II}$  and material properties are the same in each case. In all examples, tensile stresses are achieved on the bottom of the moving (right-lateral) rupture. Each plot is 6 cm x 6 cm, and stress values are given in MPa.

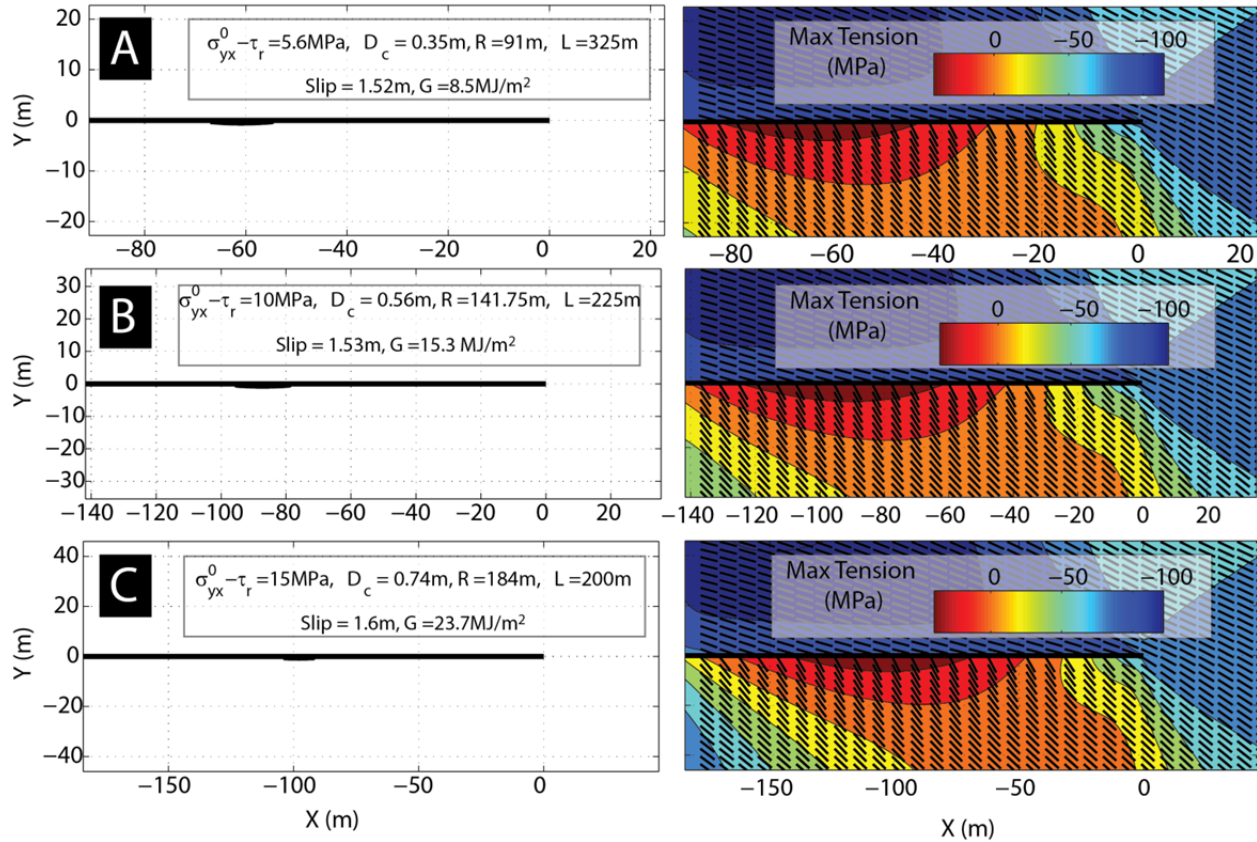


Figure DR7: Regions in which the max tensile stress exceeds critical stress  $\sigma_T = 10 \text{ MPa}$  for ruptures along the Gole Larghe Fault Zone for stress drops of 5.6MPa, 10MPa, and 15MPa as identified in Figure DR2. The right hand column are plots of maximum tensile stress fields shown in contours (units are in MPa) overlain by direction of maximum compressive stress.